Biogeosciences Discuss., doi:10.5194/bg-2016-165, 2016
Manuscript under review for journal Biogeosciences
Published: 29 April 2016

Improving vegetation phenological parameterization of a land surface model

Baozhang Chen[1,2,3] and Mingliang Che[3]

[1]Key Laboratory of Soil and Water Conservation and Desertification Combating, Ministry of Education，Beijing Forestry University, Beijing 100083，China

[2]China University of Mining and Technology, Xuzhou, and Jiangsu Center for Collaborative Innovation in Geographic Information Resource Development and Application, Nanjing, China

[3]State Key Laboratory of Resources and Environmental Information System, Institute of Geographical Sciences and Natural Resources Research, Chinese Academy of Sciences, Beijing

Correspondence to Baozhang Chen (Baozhang.Chen@igsnrr.ac.cn) and Mingliang Che (chemingliangs@163.com)

Biogeosciences Discuss., doi:10.5194/bg-2016-165, 2016
Manuscript under review for journal Biogeosciences
Published: 29 April 2016

Abstract: The growing degree day (GDD) model and the growing season index (GSI) model are two common approaches used in various land surface models (LSMs) for simulating phenophases. The capacity of these two models for simulating phenolphases was evaluated by coupling them to a LSM (DLM: Dynamic Land Model) and validated by observation data from the 22 selected eddy covariance flux towers representing six typical plant functional types. The main findings are threefold: (i) the simulated phenophases using DLM-GSI were much closer to the observations derived from the green chromatic coordinate data than using DLM-GDD. The start of the growing season (SGS) was estimated to be earlier by DLM-GSI and later by DLM-GDD. Meanwhile, the end of growing season (EGS) was estimated to be later by DLM-GSI and earlier by DLM-GDD; (ii) compared to the GDD model, the GSI model significantly decreased the absolute bias of the phenophases simulated by DLM for all sites. The DLM-GSI model simulated biases for SGS and EGS decreased by 48.2% and by 39% on average, respectively; and (iii) the accuracy of modeled GPP using the DLM-GSI model is much higher than using the DLM-GDD model for all sites. The DLM-GSI model reduced the root mean square error of simulated GPP by 8.0% and increased the corresponding index of agreement by 7.5%.

Biogeosciences Discuss., doi:10.5194/bg-2016-165, 2016
Manuscript under review for journal Biogeosciences
Published: 29 April 2016

1 Introduction

Vegetation phenology is the timing of biological events in plants that is influenced by environmental conditions, especially by long-term temperature changes (Schwartz 2013). Phenology not only reflects the seasonal alternation but also the adaptability of vegetation to environmental conditions (Che et al. 2014a). With a rapid global climate change, the phenology of vegetation has adjusted to ensure survival and reproduction (Eastman et al. 2013), and these changes have become the most sensitive indicator of climate change (Cong et al. 2012; Hamunyela et al. 2013; Menzel; Fabian 1999; Schwartz 1998). Approaches for depicting phonological changes have been recently employed in land surface models (LSMs) and have been coupled to global circulation models for estimating the effects of climate change and accounting for possible feedback (Subin et al. 2011). In LSMs, phenology is a very important module, which controls the changes and length of the growing season and influences the carbon cycle, evapotranspiration and the energy balance in the vegetation canopy (Knorr et al. 2010; Kucharik; Twine 2007; White et al. 2009). Therefore, accurately estimating phenophases in a LSM is critical to simulating the interactions between terrestrial ecosystems and climate change.

Phenological approaches in LSMs can be divided into two categories. One is satellite phenological observation, *i.e.*, the use of remotely sensed leaf area index (LAI), which describes changes in the vegetation growing season and provides a spatially integrative view of continuous biophysical states (Stöckli et al. 2008). For instance, in the community land model (CLM) (Oleson et al. 2013; Oleson et al. 2010) and the ecosystem-atmosphere simulation scheme (EASS) (Chen et al. 2007), the LAI is read directly to characterize the effects of the three-dimensional canopy structure on radiation, energy and carbon fluxes. Another is the process-based phenology model, which is embedded in LSMs either explicitly, implicitly or both. Explicit phenology models are independent of LSMs and are usually driven by offline climate factors. The growing degree day (GDD) model and the growing season index (GSI) model are the two common used representative explicit models.

The GDD model starts from Reaumur's approach, which first introduced the concept of the degree-day sum and later became referred to as the thermal time model (TM) or the spring warming model (WM) (Schwartz 2013). Chuine's approach replaced the TM model because it introduced chilling requirements in dormancy and unified various models that described the relationships between the temperature and the rate of forcing and chilling development (Chuine 2000). In Chuine's approach, the state of forcing was described as an accumulated number of the growing degree day (Murray et al. 1989), and the state of chilling was also described as an accumulated numbers of the chilling or freezing day (CD or FD). Applying the GDD and CD approaches to the initiation of leaf onset has gained considerable recognition (Arora; Boer 2005). However, this model is unable to simulate the reversible nature of the spring recovery; cold temperatures during late spring can cause growing plants to

Biogeosciences Discuss., doi:10.5194/bg-2016-165, 2016
Manuscript under review for journal Biogeosciences
Published: 29 April 2016

suffer from substantial cold damage (Arora; Boer 2005). In addition to temperature, water-stress and photoperiod are also considered important factors in vegetation phenology (Borchert et al. 2005). Studies of GDD models incorporating the effects of soil water and photoperiod have been published (Caffarra et al. 2011; Lawrence et al. 2011). Currently, GDD models were employed by many LSMs, such as the version 4 of CLM (CLM4, CLawrence et al. 2011), the biome-BGC model (Thornton; Rosenbloom 2005; Thornton et al. 2002), the integrated biosphere simulator (IBIS) (Foley et al. 1996; Kucharik 2003), the lund-potsdam-jena model (LPJ) (Sitch et al. 2000; Sitch et al. 2003) and the IAP dynamic global vegetation model (IAP-DGVM) (Zeng et al. 2014).

The GSI model combined a number of climate factors closely related to phenology, *e.g.*, temperature, light and humidity, into an index to quantify the greenness of vegetation throughout the year (Jolly et al. 2005). This approach is simple and generalized to describe phenological states on local across global scales. Furthermore, this approach is flexible enough to introduce other phenological influence factors (PIFs), as long as the relationship between the PIF and plant growing state can be reasonably described. The GSI model has not yet been employed by any published LSMs. In this study, it was coupled to a LSM (DLM : the dynamic land surface model). The DLM model was further developed by combining the algorithms embedded in EASS and CLM4 to simulate biological, geographical, physical and chemical processes (Chen et al. 2014; Chen et al. 2013) and was evolved

Biogeosciences Discuss., doi:10.5194/bg-2016-165, 2016
Manuscript under review for journal Biogeosciences
Published: 29 April 2016

into a phenology module for simulating the seasonal changes in vegetation growth.

Most studies of phenological estimates focusing on the phenology (RSP) retrieval algorithms based on remote sensing data, *e.g.*, LAI or normalized difference vegetation index (NDVI) (White et al. 2014; White et al. 2009). However, published studies that comparing process-based phenology models are limited, and researched on evaluating the phenology models coupled into LSMs are even rarer. This gap means that the validity of phenology simulation in LSMs is debatable and increases uncertainty in the estimation of carbon, water and energy exchanges in LSMs.

In this study, we compared the performance of two common used phenology models, GSI and GDD phenology models, which were coupled into DLM, focusing on two vegetation types: deciduous forest and grass. The accuracy of the phenological simulations in the two versions of DLM was evaluated against observations. Moreover, another very important variable closely related to phenology, gross primary production (GPP), was also simulated and analyzed.

2 Methods and materials

2.1 Model descriptions

2.1.1 Outline of the DLM model

The DLM model is prognostic and has been coupled to CESM 1.0.3 (Chen et al. 2014; Chen et al. 2013). DLM builds on EASS and CLM4. The main differences in algorithms among DLM, EASS, and CLM4 are shown in Table 1. DLM absorbed the

Biogeosciences Discuss., doi:10.5194/bg-2016-165, 2016
Manuscript under review for journal Biogeosciences
Published: 29 April 2016

vegetation physiological and physical algorithms based on the two-leaf canopy model, which can effectively address radiation transfer through the canopy and its impact on carbon sequestration and energy partitioning in EASS (Chen et al. 2007). DLM also employs the plant and soil biochemical processes algorithms from CLM4, which amply describe the relevant mechanisms, especially in the carbon-nitrogen (CN) biogeochemical module.

2.1.2 Phenological modules in DLM

2.1.2.1 Growing season index module

The growing season index (GSI) model uses the GSI and corresponding criteria for phenological transition stages to track all leaf phenological states and does not need to distinguish the deciduous vegetation types.

(1) Growing season index

The growing season index for triggering the leaf green-up and defoliation (Jolly et al. 2005; Stöckli et al. 2008) is expressed as:

$$GSI = f(T) \cdot f(DL) \cdot f(VPD) \tag{1}$$

where *GSI* has no unit, and its value varies from 0 to 1. The parameters $f(T)$, $f(DL)$ and $f(VPD)$ are the temperature index, the day length index and the vapor pressure deficit (VPD) index, respectively. They have no units and with values of 0~1. The statistics shows that the GSI is positively correlated with the NDVI or LAI very significantly. The temperature index $f(T)$ is calculated as,

$$f(T)=\begin{cases}0, & T \le T_{\min} \\ \dfrac{T-T_{\min}}{T_{\max}-T_{\min}}, & T_{\min} < T < T_{\max} \\ 1, & T \ge T_{\max}\end{cases} \tag{2}$$

where T, $T_{\min}$ and $T_{\max}$ are the temperature and the minimum and maximum temperature thresholds in degrees K, respectively.

The day length index $f(DL)$ is calculated as,

$$f(DL)=\begin{cases}0, & DL \le DL_{\min} \\ \dfrac{DL-DL_{\min}}{DL_{\max}-DL_{\min}}, & DL_{\min} < DL < DL_{\max} \\ 1, & DL \ge DL_{\max}\end{cases} \tag{3}$$

where DL, DL_{min} and DL_{max} are the day length and the minimum and maximum of the day length thresholds in hours, respectively.

The vapor pressure deficit index $f(VPD)$ is calculated as,

$$f(VPD)=\begin{cases}0, & VPD \ge VPD_{\max} \\ 1-\dfrac{VPD-VPD_{\min}}{VPD_{\max}-VPD_{\min}}, & VPD_{\min} < VPD < VPD_{\max} \\ 1, & VPD \le VPD_{\min}\end{cases} \tag{4}$$

where VPD, VPD_{min} and VPD_{max} are the vapor pressure deficit and the minimum and maximum VPD thresholds in *Pa*, respectively.

(2) Phenology strategy

There are four leaf phenology states in the GSI model: green-up (*i.e.*, the start of the growing season, SGS, or start of season, SOS), normal growth, defoliation and dormancy (*i.e.*, the end of the growing season, EGS, or end of season, EOS). Fig. 1 shows the corresponding method for extracting phenophases.

Biogeosciences Discuss., doi:10.5194/bg-2016-165, 2016
Manuscript under review for journal Biogeosciences
Published: 29 April 2016

Biogeosciences Discussions

At the end of vegetation dormancy, when environmental conditions become favorable to growth, the vegetation starts to emerge from dormancy and grow. To trigger vegetation green-up, the *GSI* must be smoothed by a 21-day forward moving average filter first. The moving average serves to buffer single extreme events from prematurely triggering canopy changes (Jolly et al. 2005). Then, the accumulated GSI approach for triggering the green-up is applied as follows:

$$GSIG_{sum} = \begin{cases} GSIG_{sum}^{pre} + f_{day}\,, & GSI \geq GSIG_{thr} \\ 0 \,, & GSI < GSIG_{thr} \end{cases} \tag{5}$$

where $f_{day} = Vt/86400$, Vt is time step and is equal to 1800 sec. The superscript *pre* represents the last time step. $GSIG_{sum}$ is the GSI summation for green-up in days, and $GSIG_{thr}$ has no unit for the GSI threshold for green-up.

When $GSIG_{sum} > 6$, the leaf green-up begins, and the onset counter for controlling the green-up length (t_{onset}, day) is initialized. Here, the criterion "$GSIG_{sum} > 6$" is followed by the leaf-out model in spring in Canadian terrestrial ecosystem model (CTEM) (Arora; Boer 2005). In CTEM, the leaf-out state is triggered when the net photosynthesis rate remains positive over 5-7 consecutive days. This criterion buffers single extreme events from prematurely triggering canopy changes.

During the green-up period, the onset counter t_{onset} is decremented at each time step if $GSI \geq GSIG_{thr}$ until it reaches zero, then normal growth is triggered;

$$t_{onset} = \begin{cases} t_{onset}^{pre} - f_{day}\,, & GSI \geq GSIG_{thr} \\ t_{onset}^{pre} \,, & GSI < GSIG_{thr} \end{cases} \tag{6}$$

During normal growth, the vegetation grows stably, and its LAI gradually

Biogeosciences Discuss., doi:10.5194/bg-2016-165, 2016
Manuscript under review for journal Biogeosciences
Published: 29 April 2016

reaches an annual peak. As adverse environmental conditions arrive in autumn, vegetation enters the end of normal growth (*i.e.*, the start of defoliation) when vegetation starts to drop leaves. To track leaf drop, an accumulated GSI approach is used:

$$GSID_{sum} = \begin{cases} GSID_{sum}^{pre} + f_{day}, & GSI < GSID_{thr} \\ 0, & GSI \geq GSID_{thr} \end{cases} \quad (7)$$

where $GSID_{sum}$ is the GSI summation for defoliation in days. The superscript *pre* represents the last time step. $GSID_{thr}$ has no unit and is the GSI threshold for defoliation.

When $GSID_{sum} > 6$, leaf defoliation is triggered, and the offset counter for controlling the defoliation length (t_{offset}, day) is initialized. Here, the criterion "$GSID_{sum} > 6$" uses the leaf-fall model in autumn in CTEM for reference, which triggers the leaf-fall state when the air temperature remains below a certain temperature threshold for 5-7 consecutive days. This criterion serves to buffer single extreme events from prematurely triggering canopy changes.

During the defoliation period, the offset counter t_{offset} is decremented at each time step if $GSI < GSID_{thr}$ until it reaches zero, and then dormancy is triggered;

$$t_{offset} = \begin{cases} t_{offset}^{pre} - f_{day}, & GSI < GSID_{thr} \\ t_{offset}^{pre}, & GSI \geq GSID_{thr} \end{cases} \quad (8)$$

2.1.2.2 Growing degree day module

The growing degree day (GDD) model was originated from CLM4. From the

Biogeosciences Discuss., doi:10.5194/bg-2016-165, 2016
Manuscript under review for journal Biogeosciences
Published: 29 April 2016

modularization viewpoint, the GDD model is independent of CLM4, so the GDD model was easy to couple into other LSMs, e.g., the DLM model. Two deciduous vegetation types are contained in the GDD model. One is seasonally deciduous, and the other is stress-deciduous. The former refers to the temperate and boreal deciduous trees; the latter includes temperate and boreal deciduous shrubs, grass and tropical deciduous trees. The phenophases in this model also contain green-up, normal growth, defoliation and dormancy, which are assumed to be only driven by climate factors (*e.g.*, temperature and soil water) and day length.

(1) Seasonal-Deciduous Phenology

Green-up for seasonal-deciduous vegetation is triggered based on an accumulated GDD approach (White et al. 1997). The GDD summation (GDD_{sum}, degree·day) is initiated at zero when the phenological state is dormant and the model time step crosses the winter solstice (Oleson et al. 2013). Once the environmental conditions are met, GDD_{sum} is updated at each time step as:

$$GDD_{sum} = \begin{cases} GDD_{sum}^{pre} + (T_{soil} - 273.15) \cdot f_{day}, & T_{soil} > 273.15 \\ GDD_{sum}^{pre}, & T_{soil} \le 273.15 \end{cases} \tag{9}$$

where $f_{day} = \nabla t / 86400$, ∇t is time step and equals 1800 sec. The superscript *pre* represents the last time step. T_{soil} is the temperature of the third soil layer in K. When GDD_{sum} is greater than the GDD summation threshold (GDD_{thr}, degree·day), green-up is triggered, and the onset counter (t_{onset}, day) that controls the green-up length is initialized. The GDD_{thr} is estimated as follows:

Biogeosciences Discuss., doi:10.5194/bg-2016-165, 2016
Manuscript under review for journal Biogeosciences
Published: 29 April 2016

$$GDD_{thr} = \exp(4.8 + 0.13 \cdot (T_{air} - 273.15)) \tag{10}$$

where T_{air} is the annual average air temperature at a 2 m height in degrees K.

During green-up, the onset counter (t_{onset}) is decremented at each time step until it reaches zero, triggering normal growth,

$$t_{onset} = t_{onset}^{pre} - f_{day} \tag{11}$$

After simulating time past the summer solstice, vegetation defoliation is triggered if the day length (DL, hr) is shorter than the corresponding threshold (DL_{thr}, hr), and the offset counter (t_{offset}, day) that controls the defoliation length is initialized at the beginning of the defoliation period.

During defoliation, the offset counter t_{offset} decreases at each time step until it reaches zero, triggering dormancy,

$$t_{offset} = t_{offset}^{pre} - f_{day} \tag{12}$$

(2) Stress-Deciduous Phenology

The process for triggering green-up of stress-deciduous vegetation is more complex than for the seasonally deciduous vegetation in CLM4. It is influenced by temperature, soil water and day length simultaneously.

First, the freezing day accumulator for green-up (FDG_{sum}, day) is necessary and is calculated as:

$$FDG_{sum} = \begin{cases} FDG_{sum}^{pre} + f_{day}, & T_{soil} < 273.15 \\ FDG_{sum}^{pre}, & T_{soil} \geq 273.15 \end{cases} \tag{13}$$

where $f_{day} = \mathrm{V}t / 86400$, $\mathrm{V}t$ is time step and set to be 1800 sec. The superscript *pre*

Biogeosciences Discuss., doi:10.5194/bg-2016-165, 2016
Manuscript under review for journal Biogeosciences
Published: 29 April 2016

represents the last time step. FDG_{sum} is initialized to zero at the beginning of the dormant period. T_{soil} is the temperature of the third soil layer in K.

If $FDG_{sum} > FDG_{thr}$, where FDG_{thr} is the freezing day summation threshold for green-up in days, the growing-degree-day summation (GDD_{sum}, degree·day) (see Eq. 9) is followed exactly.

Meanwhile, the accumulated soil water index for green-up ($SWIG_{sum}$, days) is calculated as:

$$SWIG_{sum} = \begin{cases} SWIG_{sum}^{pre} + f_{day}, & \Psi_{soil} \geq \Psi_{onset} \\ SWIG_{sum}^{pre}, & \Psi_{soil} < \Psi_{onset} \end{cases} \quad (14)$$

$SWIG_{sum}$ is initialized to zero at the beginning of a dormant period, Ψ_{soil} is the soil water potential in the third soil layer in MPa, and Ψ_{onset} is the soil water potential threshold for green-up in MPa.

Only if $GDD_{sum} > GDD_{thr}$ (or T_{soil} is always greater than 273.15K) and $SWIG_{sum} > SWIG_{thr}$ and $DL > DL_{thr}$ is green-up triggered, where GDD_{thr} is the GDD summation threshold in degree·days (see Eq. 10), the $SWIG_{thr}$ is the soil water index summation threshold in days, DL is the day length in hours, and DL_{thr} is the day length threshold in hours.

At the beginning of the green-up period, an onset counter for controlling the green-up length (t_{onset}, days) is initialized. Then, t_{onset} is decremented at each time step until it reaches zero, triggering normal growth (see Eq. 11).

During normal growth, any one of the following unfavorable conditions is

Biogeosciences Discuss., doi:10.5194/bg-2016-165, 2016
Manuscript under review for journal Biogeosciences
Published: 29 April 2016

sufficient to trigger vegetation defoliation - a sustained period of dry soil, a sustained period of cold temperature, or a shorter day length.

The dry soil condition is evaluated with the soil water index accumulator for defoliation ($SWID_{sum}$, day), which is expressed as:

$$SWID_{sum} = \begin{cases} SWID_{sum}^{pre} + f_{day} & , \quad \Psi_{soil} \le \Psi_{offset} \\ \max(SWID_{sum}^{pre} - f_{day}, 0), & \quad \Psi_{soil} > \Psi_{offset} \end{cases} \tag{15}$$

where Ψ_{offset} is the soil water potential threshold for defoliation in MPa.

Meanwhile, the cold temperature condition is calculated with the freezing day accumulator for defoliation (FDD_{sum}, day) and is described as:

$$FDD_{sum} = \begin{cases} FDD_{sum}^{pre} + f_{day} & , \quad T_{soil} \le 273.15 \\ \max(FDD_{sum}^{pre} - f_{day}, 0), & \quad T_{soil} > 273.15 \end{cases} \tag{16}$$

When $SWID_{sum}$ > $SWID_{thd}$ or FDD_{sum} > FDD_{thr} or DL<DL_{thr}, defoliation is triggered. $SWID_{thr}$ is the soil water index summation threshold for defoliation in days and FDD_{thr} is the freezing day accumulator threshold for defoliation in days.

The offset counter for controlling the defoliation length (t_{offset}, days) is initialized and decreases at each time step until it reaches zero, triggering dormancy (see Eq. 12).

2.2 Data sets used

2.2.1 FLUXNET Data

The selected 22 eddy-covariance (EC) sites from the FLUXNET database (http://fluxnet.ornl.gov/) are mainly distributed in North America and Europe (see Fig. 2). The EC sites were selected according to the following requirements: (i) the dominant vegetation type at the site was limited to deciduous forest, deciduous shrubs and grass; (ii) the site provided at least four years of continuous data as a part of a publicly accessible standardized Level 3 or 4 database; (iii) a 'site-year' was accepted for analysis if more than 90% of the half hours in a year contained non-missing values for the meteorological data and the carbon flux data (Chen et al. 2013); and (iv) the sites represented as many climate zones as possible.

The final selected sites were expected to represent the following four main climatic environments including temperate, boreal, arid and the moist climate zones and four biome types containing needleleaf deciduous forests (NDF), broadleaf deciduous forests (BDF), broadleaf deciduous shrubs (BDS) and grasslands. Different biome types in a particular climate environment are usually characterized by different leaf types, leaf longevity and life forms (Roth et al. 2015). Thus, a biome type located in a particular climate zone can represent the corresponding plant function type (PFT). A description of the information for the selected sites classified by PFT can be found in Table 2.

Every site contained half-hourly meteorological and GPP data for 4 consecutive years. The data for the first two consecutive years were used to optimize the model parameters and for the next two consecutive years to evaluate the simulation results of DLM. Meteorological data including down-welling solar radiation, precipitation, wind speed, air temperature and relative humidity were applied to drive DLM. The EC-measured GPP data were used for model calibration and assessment.

Biogeosciences Discuss., doi:10.5194/bg-2016-165, 2016
Manuscript under review for journal Biogeosciences
Published: 29 April 2016

2.2.2 GPP and phenology data

GPP data usually have gaps. If the gaps were less than 2 hours, the missing values were filled by piecewise linear interpolation. To fill longer gaps, the light use efficiency (LUE) model was employed (Monteith 1972; Sims et al. 2008). Though other uncertainties still existed in the EC-measured GPP, *e.g.*, underestimation of the ecosystem respiration at night (Schaefer et al. 2012), they were still regarded as the 'ground truth' in this study.

The phenological observations used for evaluating the simulated phenophases of DLM contained two parts. One part was derived from the EC-measured GPP, and the other was derived from the observed green chromatic coordinate (GCC) data.

The phenological inversion method based on the GPP data used the ratio of the daily GPP to the growing season amplitude to identify the phenophases (Melaas et al. 2013), which only retrieved the start of the growing season and the end of the growing season.

The GCC data were derived from the digital images photographed by an automated and high-frequency digital camera that is generally applied in modern phenological observation (Ide; Oguma 2010) and were calculated from the average red (R), green (G), and blue (B) pixel digital numbers (DNs) over the region of interest (ROI), *i.e.*, GCC = G/(G+R+B) (Ahrends et al. 2008; Ahrends et al. 2009; Sonnentag et al. 2012). Quality control of the GCC data was necessary to correct for

Biogeosciences Discuss., doi:10.5194/bg-2016-165, 2016
Manuscript under review for journal Biogeosciences
Published: 29 April 2016

gaps and false data before using a smoothed curve for fitting, following the approach of Ludvig *et al.*(Ludvig 2014). The inflection points of the curve were calculated to identify the phenophases. The general smoothed curves contained the loGSItic function, the double-loGSItic function, the Asymmetric Gaussian function, *etc*. (Ide; Oguma 2010; Klosterman et al. 2014). Some studies indicated the Scurve function describing the vegetation growing state better than the loGSItic function and the Asymmetric Gaussian function (Che et al. 2014a; Che et al. 2014b). Thus, the Scurve function was used here to fit the GCC data, and the corresponding process for extracting phenophases based on the Scurve function was carried out. The final inversion phenophases included the start of the growing season, normal growth, defoliation and the end of the growing season. Simultaneously, visual interpretation of the digital images was also used to appropriately correct the retrieved results. The digital images were downloaded from the PhenoCam Network (http://phenocam.sr.unh.edu/webcam/). Considering the geographic position and the site-year of the flux sites, after selection, the PhenoCam sites only contained the US-MOz site (*i.e.*, the Columbiamissouri site). Fig. 3 shows the digital images for key phenophases at this site. The plants started to green-up in early April (Fig. 3a) and entered into normal growth in the middle of May (Fig. 3b). Leaves began to fall widely in later October (Fig. 3c), and dormancy began in the middle of November (Fig. 3d).

Admittedly, certain uncertainties existed in the two phenological observations.

Biogeosciences Discuss., doi:10.5194/bg-2016-165, 2016
Manuscript under review for journal Biogeosciences
Published: 29 April 2016

For example, the retrieval phenophases of the GPP were deeply affected by the quality itself. The GPP ratio method was a dynamic threshold method. Before using it, the GPP data were first smoothed by the cubic spline. Even so, this method was still sensitive to high GPP values occurring in early spring or later autumn. If the GPP high values were noisy, the retrieval phenophases would have large uncertainties. The GCC data might be distorted at a certain time due to the effect of camera firmware, the white balance setting, changes in illumination and smog, etc. (Ahrends et al. 2008; Ide; Oguma 2010). Furthermore, delimiting the ROI of the image and using the phenology inversion method might affect the accuracy of the phenological inversion results (Ahrends et al. 2009; Klosterman et al. 2014). However, if the ground measured phenological observations were absent, the retrieval phenophases based on the GPP and GCC data were still considered as the 'observed values' for model evaluation.

2.3 Model suns and parameters optimization

2.3.1 Model control tests and runs

To evaluate the performance of the two alternative phenology models coupled to DLM, a control test was designed. Based on DLM, two versions of the model were built by coupling the GSI and GDD models, respectively, which are designated as DLM-GSI and DLM-GDD.

Through the control test, the accuracy of simulating phenophases using the two versions of DLM can be objectively assessed. Additionally, the effects of the phenology models on GPP simulated using the two versions can be evaluated.

We ran separately the two DLM versions (DLM-GSI and DLM-GDD) at half-hourly time steps with the same observed meteorological and land surface data as inputs. Missing meteorological data were supplied by linear interpolation for gaps of less than 2 hours (Chen et al. 2013). Various methods were used for filling longer gaps for different variables. For variation trends of the down-welling solar radiation and air temperature, the sine function was appropriate. For relative humidity, the cosine function was suitable. Considering their strong randomness, the piecewise linear interpolation approach was used for precipitation and wind speed.

The soil texture (*i.e.*, percentages of sand and clay) was obtained from the site information or published articles. Other soil property data were obtained from CESM1.0.3 as a source of land surface data for the year 2000 (Lawrence et al. 2011). The soil state variables (*e.g.*, soil temperature and moisture) and vegetation state variables (*e.g.*, LAI, stem area index (SAI) and canopy top and bottom heights) at each site for the off-line simulations were obtained from the initialization. The initialization was acquired from a long (at least 2000 years) spin-up simulation until the carbon and nitrogen pools and associated LAI, SAI, and vegetation heights approximated the equilibrium with the repeating atmospheric forcing data for the years of 1972-2001 (Qian et al. 2006) provided by NCAR. The CO_2 concentration, nitrogen and aerosol deposition at year 2000 levels at each site were also provided by NCAR.

2.3.2 Parameters optimization

The PFT-dependent parameters for vegetation physiology, *e.g.*, the leaf maximum carboxylation rate at 25 °C and the leaf stomatal resistance-to-photosynthesis relationship in DLM, were slightly adjusted based on published parameters (Chen et al. 2013). The foliage clumping index in DLM was taken from published papers (Chen et al. 2007; Chen et al. 2013).

The parameters in the GSI phenological modules were initialized by referring to literatures (Jolly et al. 2005; Stöckli et al. 2008). These phenological parameters were further optimized based on EC-measured GPP using the simulated annealing (SA) algorithm (Dong et al. 2013; Li et al. 2004), which was not only independent of the cost function but also able to produce global optimal parameters of the model. The final optimized parameters of the GSI model can be found in Table 3.

The parameters in the GDD phenological model were designed to be independent of the PFTs and originated from the CLM4 technical manual (Oleson et al. 2013; Oleson et al. 2010). The final parameters are as follows: N_{onset} = 30 day, N_{offset} = 15 day, FDG_{thr} = 15 day, FDD_{thr} = 15 day, Ψ_{onset} = -2 MPa, Ψ_{offset} = -2 MPa, $SWIG_{thr}$ = 15 day, $SWID_{thr}$ = 15 day, DL_{thr}= 11 hr, where N_{onset} is the initialized onset counter for controlling the length of green-up, N_{offset} is the initialized offset counter for controlling the length of defoliation, FDG_{thr} is the freezing day summation threshold for green-up, FDD_{thr} is the freezing day summation threshold for defoliation, Ψ_{onset} is the soil

Biogeosciences Discuss., doi:10.5194/bg-2016-165, 2016
Manuscript under review for journal Biogeosciences
Published: 29 April 2016

water potential threshold for green-up, Ψ_{offset} is the soil water potential threshold for defoliation, $SWIG_{thr}$ is the soil water index summation threshold for green-up, $SWID_{thr}$ is the soil water index summation threshold for defoliation, and DL_{thr} is the day length threshold.

2.4 Model evaluation methods

For assessing the model performance, statistical analyses containing bias (Eq. 17), absolute bias (Eq. 18), root mean square error (RMSE, Eq. 18) and index of agreement (IA, Eq. 19) were used (Willmott 1982).

$$Bias = \frac{1}{n}\sum_{i=1}^{n}(P_i - O_i)\ , \tag{17}$$

$$ABias = \frac{1}{n}\sum_{i=1}^{n}|\ P_i - O_i\ |\ \ , \tag{18}$$

$$RMSE = \sqrt{\frac{1}{n}\sum_{i=1}^{n}(P_i - O_i)^2}\ , \tag{19}$$

$$IA = 1 - \frac{\sum_{i=1}^{n}(P_i - O_i)^2}{\sum_{i=1}^{n}(|\ P_i - \overline{O}\ | + |\ O_i - \overline{O}\ |)^2} \tag{20}$$

where P is the model simulated value, O is the observed value, $\overline{O}$ is the observed mean, and i and n represent the sequence number and the total number of data points, respectively.

3 Results

3.1 Simulation of phenological events

First, the simulated phenophases using DLM-GSI and DLM-GDD were compared with observations derived from the GCC data at the US-MOz site (Fig. 4). A comparison of corresponding phenological absolute biases (Abias) can be found in Fig. 5. Both of two versions of DLM simulated the phenophases well at this site. However, the differences in the simulated phenophases were also evident.

The simulated start of growing season derived from DLM-GSI and DLM-GDD were earlier and later than the observed values, respectively. The Abias of the DLM-GSI was 3 days less than that of DLM-GDD on average. The difference between the simulated normal growth phenophases using the two versions of DLM was also obvious. The DLM-GSI estimated the phenophase earlier, but the DLM-GDD estimated it later. The Abias of the former was 4 days less than that of the latter on average. For defoliation, Both DLM-GSI and DLM-GDD estimated the phenophase earlier, but the former had a lower prior-estimation error (Abias = 4days) than the latter (Abias = 8days). For the EGS simulation, the results of DLM-GSI and DLM-GDD were later and earlier than the observed values, respectively, and the EGS Abias of DLM-GSI was 5 days less than DLM-GDD.

The above analysis indicates the simulated phenophases of DLM-GSI were much closer to observed values than those of DLM-GDD, and the DLM-GSI estimated SGS

Biogeosciences Discuss., doi:10.5194/bg-2016-165, 2016
Manuscript under review for journal Biogeosciences
Published: 29 April 2016

and EGS earlier and later, respectively, but DLM-GDD did the opposite.

The simulation performance of two versions of DLM was assessed by using observations derived from the EC-measured GPP at all sites. A comparison of the phenophases simulated by the two versions of DLM and the observed values is shown in Fig. 6. In this study, we focused on the start of the growing season (Fig. 6a) and the end of the growing season (Fig. 6b) at the EC sites. A corresponding comparison of the absolute biases for the simulated phenophases is shown in Fig. 7.

As shown in Figs. 6 & 7, the differences between the phenophases simulated by the two versions of DLM were remarkable, and the differences also existed for each plant function type. In Fig. 8, the boxplot shows the discrete character of the absolute biases for the simulated results by using the two versions for each PFT. For boreal needleleaf deciduous forest (BNDF) (Figs. 8a_1 & 8b_1), the Abias range and interquartile range of the simulated SGS using DLM-GSI were both lower than those simulated using DLM-GDD, as were the mean and median of the SGS Abiases. The Abias range, mean and median of the simulated EGS using DLM-GSI were all lower than those of DLM-GDD, but the Abias interquartile range was higher. At the BNDF sites, the accuracy of the phenophases simulated using DLM-GSI at the CA-NS1 site and the FI-Hyy site was obviously higher than those simulated using DLM-GDD. The results showed that the GSI model reduced the SGS and EGS Abiases of DLM at the CA-NS1 site by 6 and 30 days, respectively. As the same time, the GSI model reduced the SGS and EGS Abiases of DLM at the FI-Hyy site by 29 days and 8 days,

Biogeosciences Discuss., doi:10.5194/bg-2016-165, 2016
Manuscript under review for journal Biogeosciences
Published: 29 April 2016

respectively.

For temperate broadleaf deciduous forest (TBDF) (Figs. 8a$_2$ & 8b$_2$), the Abias range and interquartile range of the SGS simulated by DLM-GSI were both shorter than those of DLM-GDD, as were the mean and median of SGS Abiases. The Abias range of EGS simulated by DLM-GSI was consistent with that simulated by DLM-GDD. The Abias mean and median of simulated EGS using DLM-GSI were slightly lower than the values obtained using DLM-GDD, but the interquartile range was higher for DLM-GSI compared with DLM-GDD. At the TBDF sites, the simulated results using DLM-GSI at the CH-Lae site and the US-MOz site were much closer to observed values than using DLM-GDD. The results showed that the GSI model reduced the SGS and EGS Abiases of DLM at the CH-Lae site by 32 days and 21 days, respectively. At the same time, the accuracy of simulated SGS using DLM-GSI at the FR-Fon site and the IT-Col site was also higher than that of using DLM-GDD. However, the accuracy of simulated EGS using DLM-GSI was lower than that of using DLM-GDD. At the US-Los site, the accuracy of simulated phenophases using DLM-GSI was inferior to DLM-GDD.

For the boreal broadleaf deciduous forest (BBDF) (Figs. 8a$_3$ & 8b$_3$), the Abias range and interquartile range of simulated SGS using DLM-GSI were both less than using DLM-GDD, as were the mean and median of SGS Abiases. The Abias range, mean and median of simulated EGS uisng DLM-GSI were all lower than using DLM-GDD, but the Abias interquartile range was higher for DLM-GSI compared with

DLM-GDD. At the BBDF sites, the accuracies of simulated phenophases using DLM-GSI exceeded those of using DLM-GDD largely, especially for the DE-Gri site, the DK-Sor site and the BE-Vie site. The results showed that the GSI model reduced the SGS and EGS Abiases uisng DLM at the DE-Gri site by 28 and 7 days, respectively.

For the temperate and boreal broadleaf deciduous shrubs (BDS) (Figs. $8a_4$, $8b_4$, $8a_5$ & $8b_5$), the Abias range and interquartile range of simulated SGS and EGS using DLM-GSI were all lower than those using DLM-GDD, as were the Abias mean and median. At the BDS sites, the accuracy of simulated phenophases using DLM-GSI was higher than using DLM-GDD widely, especially for the US-Fwf site and the CA-NS6 site. The results showed that the GSI model reduced the SGS and EGS Abiases of DLM at the CA-NS6 site by 17 and 58 days, respectively. At the US-Ivo site, the simulated phenophases using DLM-GSI were consistent with using DLM-GDD.

For temperate grass (Figs. $8a_6$ & $8b_6$), the Abias range of modeled SGS using the two versions of DLM were both broad, but the Abias interquartile range, mean and median of simulated SGS using DLM-GSI were all shorter than using DLM-GDD. However, the Abias range and interquartile range of simulated EGS using DLM-GSI were both narrower than using DLM-GDD, as were the EGS Abias mean and median. Compared to the general accuracy of simulated phenophases using both two versions of DLM for all sites (Figs. $8a_7$ & $8b_7$), the phenological Abias range and interquartile range of using DLM-GSI were both shorter than using DLM-GDD, as were the Abias mean and median. At the grass sites, the phenological accuracy of the DLM-GSI was generally higher than that of using DLM-GDD. Nevertheless, the GSI model indistinctively increased the EGS accuracy of using DLM at the PT-Mi2 site and US-Wkg site.

The above analysis indicates that the Abias range and interquartile range of using DLM-GSI were both shorter, and the Abias mean and median were both lower, showing that the simulated results of DLM-GSI were more stable and reasonable than those using DLM-GDD. The GSI model significantly decreased the Abias of the phenophases simulated by the DLM compared to using the GDD model. By using the GSI model, the Abias of SGS simulated using DLM decreased by 48.2% on average while the Abias of EGS declined by 39.6%.

3.2 GPP simulations

A comparison of simulated GPP using DLM-GSI and DLM-GDD with the observed values is shown in Fig. 9. The corresponding root mean square errors (RMSEs) and indices of agreement (IA) for GPP simulation are shown in Fig. 10. By adopting different phenology models under conditions for which the phenophase could be estimated, DLM can simulate daily GPP well. The simulated GPP using DLM-GSI was consistent with DLM-GDD. However, the differences between simulated GPP were also quite obvious for each PFT and at each site.

Biogeosciences Discuss., doi:10.5194/bg-2016-165, 2016
Manuscript under review for journal Biogeosciences
Published: 29 April 2016

Table 4 shows RMSE and IA of simulated GPP using the two versions of DLM for different PFTs. Obviously, DLM-GSI had lower RMSEs and higher IAs compared to DLM-GDD for all PFTs. For the PFTs of the TBDS, the BBDS and the temperate grass, the GPP RMSE of using DLM-GSI was lower than using DLM-GDD by at least 15%. The GPP IA of using DLM-GSI was higher than using DLM-GDD by at least 12%. The GSI model sharply improved the accuracy of simulated GPP by using DLM for these PFTs. For the PFT of BNDF, the GPP RMSE of using DLM-GSI was lower thanusing DLM-GDD by 6.4%, and the GPP IA exceeded it by 3.9%. The GSI model clearly improved the accuracy of simulated GPP by using DLM. For the PFTs of TBDF and the BBDF, the GSI model slightly improved the accuracy of simulated GPP with DLM compared to using GDD model, decreasing the GPP RMSE of uisng DLM by only 2.0% - 3.5% and increasing the corresponding IA by only 0.4% - 1.8%.

At the BNDF sites, the GSI model sharply improved the accuracy of simulated spring GPP using DLM at the CA-NS1 site and the FI-Hyy site and also obviously improved the accuracy of simulated autumn GPP using DLM at the CA-NS1 site. The results showed the GSI model reduced the simulated GPP RMSE of using DLM in spring at the FI-Hyy site by 36.5% and increased the corresponding IA by 75.9%. At the TBDF sites, the GSI model significantly improved the accuracy of simulated spring GPP using DLM at the CH-Lae site. The GSI model decreased the GPP RMSE of using DLM in spring at this site by 19.1% and increased the corresponding IA by 20.2%. For the other TBDF sites, a lesser improvement of simulated GPP accuracy by

Biogeosciences Discuss., doi:10.5194/bg-2016-165, 2016
Manuscript under review for journal Biogeosciences
Published: 29 April 2016

the GSI model using DLM in the growing season was noted. At some sites, the accuracy of simulated GPP based on the GSI model was lower than for the GDD model. At the BBDF sites, the GSI model sharply improved simulated GPP accuracy of using DLM at the DK-Sor site, the BE-Vie site and DE-Gri site. The GSI model reduced the GPP RMSE of using DLM in spring at the DK-Sor site by 29.5% and increased the corresponding IA by 85.0%. The GSI model also decreased the autumn GPP RMSE of using DLM at this site by 7.5% and increased the corresponding IA by 4.3%. At the DE-Hai site, the estimated SGS and EGS using DLM-GSI was respectively earlier and later compared to the observed values. The Abiases for the SGS and EGS of using DLM-GSI were both higher than using DLM-GDD. Thus, the GPP results simulated using DLM-GSI were inferior to DLM-GDD at this site. At the TBDS sites, the GSI model significantly improved the accuracy of simulated GPP using DLM at the CA-Mer site and the US-Fwf site. Meanwhile, the GSI model obviously improved the accuracy of simulated spring GPP using DLM at the US-Ton site. The results showed the RMSE of simulated spring GPP using DLM-GSI at the CA-Mer site was lower than using DLM-GDD by 17.5%, and the corresponding IA was higher by 20.5%. The RMSE of simulated autumn GPP using DLM-GSI at this site was lower than using DLM-GDD by 3.8%, and the corresponding IA was higher by 4.1%. At the BBDS sites, the GSI model significantly improved the accuracy of GPP simulated using DLM at the CA-NS6 site and the US-Ivo site. At the temperate grass sites, the GSI model also significantly improved the accuracy of GPP simulated

Biogeosciences Discuss., doi:10.5194/bg-2016-165, 2016
Manuscript under review for journal Biogeosciences
Published: 29 April 2016

using DLM at most sites.

From the above analysis, the GSI model significantly improved the accuracy of simulated GPP in DLM for different PFTs compared to the GDD model. For most of the sites, the RMSEs of simulated GPP using DLM-GSI were lower than using the DLM-GDD model, and the IA was on the contrary, especially for GPP simulation in spring and autumn. Over all, the GSI model increased the accuracy of GPP simulation by using DLM compared to using the GDD model. The GSI model reduced the GPP RMSE of using DLM by 8.0%, and increased the corresponding IA by 7.5%.

4 Discussions

According to the characteristics of climate zones, the sites can be divided into a moist climate zone and an arid climate zone. Summarizing accuracies of simulated phenophases for these two kinds of sites showed that the Abias range and interquartile range of the phenophases simulated using DLM-GSI and DLM-GDD for the moist climate sites were less broad than those for the arid climate sites, as were the Abias mean and median. For example, the Abias interquartiles for the SGS simulated using DLM-GSI for the moist and arid climate sites were 18 and 24 days, respectively, and the Abias interquartiles for the EGS simulated using DLM-GSI for the moist and arid climate sites were 10 and 15 days, respectively. Meanwhile, the Abias interquartiles for the SGS simulated using DLM-GDD for the moist and arid climate sites were 22 and 59 days, respectively, and the Abias interquartiles for the EGS simulated using

Biogeosciences Discuss., doi:10.5194/bg-2016-165, 2016
Manuscript under review for journal Biogeosciences
Published: 29 April 2016

DLM-GDD at the moist and arid climate sites were 10 and 27 days, respectively. Thus, the accuracies of the phenophases simulated with the phenology models for the moist climate sites were higher than for the arid climate sites. At the temperate arid sites, the effect of moisture on the vegetation phenology is second important compared to that of temperature. In the warm temperate arid sites, the importance of water was even greater than that of temperature. Fig. 11 shows the effect of the sensitivities of the phenology parameters on the growing season index at the US-Wkg site. The sensitivities of temperature and vapor pressure deficit were both important to the growing season index. However, the effect of the temperature sensitivity (see the error bars in light red in Fig. 11) on the growing season index was confined to the outside of the growing season (see the green dashed line derived from the EC-measured GPP in Fig. 11). The effect of VPD sensitivity (see the error bars in light blue in Fig. 11) on the growing season index was mainly located in the growing season. That is to say, at the US-Wkg site, the adjustment of temperature parameters made little contribution to improving the accuracy of the phenophases simulated by the GSI model, but the adjustment of VPD parameters was on the contrary. Nevertheless, the accurate acquisition of VPD parameters at this site was not easy. In addition, the parameters used in this study for simulating the phenophases were calculated from the average parameters at different sites for which the PFT was the same. Even if the precise VPD parameters could be obtained at this site, the uncertainty was still large when the values were averaged.

Biogeosciences Discuss., doi:10.5194/bg-2016-165, 2016
Manuscript under review for journal Biogeosciences
Published: 29 April 2016

Furthermore, the GPP observations at the US-Wkg site (Fig. 9v) indicated that the growing seasons were bimodal. The VPD parameters and the threshold parameters for triggering the phenophases used in the GSI model were all constant. This scheme could lead to a certain bias when the GSI model was used to simulate phenophases at the sites at which the number of growing seasons was greater than one. This also occurred at the temperate arid sites, such as the PT-Mi2 and the US-Ton sites. The statistics showed that the accuracy of the phenophases simulated with DLM-GSI and DLM-GDD at the single-season vegetation sites was higher than at the multi-season vegetation sites.

For example, the bias of phenophases simulated using DLM-GDD at the US-Wkg site was large. The annual average air temperature was approximately 17.25 ºC at the US-Wkg site, and the annual minimum temperature (-3 ºC) occurred in winter. Similar to the GSI model, the effect of temperature on triggering the phenophases for the GDD model was weak at this site. The annual precipitation was approximately 245.78 mm at this site. The sparse precipitation was the main factor controlling the vegetation phenology. The GDD model estimated the SGS and the EGS by calculating the cumulative days when the soil water potential (SWP) was higher or lower than -2 MPa, but the starting dates when the SWP estimated using DLM-GDD continuously exceeded -2 MPa in 2006 were April 19 and July 20. In fact, the simulated SWP using DLM was inconsistent with the observed values for both days, causing large biases in the phenophases simulated using DLM-GDD compared

Biogeosciences Discuss., doi:10.5194/bg-2016-165, 2016
Manuscript under review for journal Biogeosciences
Published: 29 April 2016

to the observed values. The SWP variable was a derivative in DLM. For that reason, the adoption of the derivative variables by the GDD model to simulate the phenophases was not ideal. Similar to the GSI model, the threshold parameters (*e.g.*, the threshold of SWP) in the GDD model were constant and were also deficient for phenophase simulation at the multi-season vegetation sites. The defective model structure and uncertainty in parameters caused the simulated phenophases using the GDD model to have large biases at other sites (*e.g.*, the PT-Mi2 site and the US-FPe site).

Compared to the observed values, the Abiases of simulated phenophases using the two versions of DLM were significant, although the Abiases of using DLM-GSI were comparatively less, indicating that the two phenology models still must be further developed and perfected by future studies. In addition, the DLM must also be improved, particularly by obtaining more accurate simulated variables as inputs for the phenology models.

5 Conclusion

The two different phenological schemes, the GSI and the GDD models, were coupled to DLM and were evaluated for deciduous forests and grasses against the observed phenology. Through control tests, the simulated phenophases and GPP by the two versions of DLM were analyzed and compared. The main conclusions are as follows:

Biogeosciences Discuss., doi:10.5194/bg-2016-165, 2016
Manuscript under review for journal Biogeosciences
Published: 29 April 2016

(i) Compared with the phenological observations derived from the GCC data at the US-MOz site, DLM-GSI had lower absolute biases for estimating the phenophases including the start of the growing season, normal growth, defoliation and the end of the growing season compared to DLM-GDD. The simulated phenophases using DLM-GSI were much closer to the observed values than those using DLM-GDD at this site. The start of the growing season was estimated earlier using DLM-GSI but later using DLM-GDD at the US-MOz site. Meanwhile, the end of growing season was estimated later using DLM-GSI but earlier using DLM-GDD.

(ii) By comparing against the phenological observations derived from the GPP data at all sites, the absolute bias of the phenophases simulated using DLM-GSI had a tighter range and interquartile range than using DLM-GDD and a lower mean and median than using DLM-GDD for various PFTs, indicating that the simulated results of using DLM-GSI were more stable and reasonable than using DLM-GDD. Overall, the GSI model significantly decreased the absolute bias of the phenophases simulated using DLM at all sites compared to the GDD model. Additionally, the use of the GSI model decreased the absolute bias of the SGS simulated using DLM by 48.2% on average and the absolute bias of the EGS declined by 39%.

(iii) The GSI model significantly improved the accuracy of the GPP simulated using DLM compared to the GDD model for various PFTs. For most of the sites, the RMSE of simulated GPP using DLM-GSI was lower than that of using DLM-GDD, and the IA was higher using DLM-GSI than using DLM-GDD, especially for GPP simulation in spring and autumn. Over all, the GSI model improved the accuracy of GPP simulation using DLM compared with using the GDD model at all sites. The GSI model reduced the simulated GPP RMSE of the DLM model by 8.0% and increased the corresponding IA by 7.5%.

Acknowledgements. This research was financially supported by a research grant (2013BAC03B04) of National Key Technology Support Program and a research grant (41271116) funded by the National Science Foundation of China, a research grant (2012ZD010) of the Key Project for the Strategic Science Plan in Institute of Geographic Sciences and Natural Resources Research, Chinese Academy of Sciences (CAS), and Jiangsu Provincial 'double creation' program. We acknowledge the agencies that supported the operations at the flux towers used here, which are parts of FLUXNET (http://fluxnet.ornl.gov/). We thank the PhenoCam Network for making the phenology imagery freely available for download (http://phenocam.sr.unh.edu/). We thank Dr. Huifang Zhang, Dr. Jing Chen, Dr. Xianming Dou, Ms.Yuchen Wang, Ms. Xiaofeng Lin and Mr. Shaobo Sun of IGSNRR for downloading and gap-filling FLUXNET data.

Biogeosciences Discuss., doi:10.5194/bg-2016-165, 2016
Manuscript under review for journal Biogeosciences
Published: 29 April 2016

Tables caption

Table 1. An algorithmic comparison among EASS, CLM4 and DLM.

Table 2. Descriptions of global FLUXNET sites used.

Table 3. Phenological parameters in the DLM-GSI model.

Table 4. Comparison of the root mean square error (RMSE) and the index of agreements (IAs) for gross primary production simulation for different vegetation types using the DLM-GSI and DLM-GDD models.

Biogeosciences Discuss., doi:10.5194/bg-2016-165, 2016
Manuscript under review for journal Biogeosciences
Published: 29 April 2016

Biogeosciences Discussions Open Access EGU

Table 1. An algorithmic comparison among EASS, CLM4 and DLM.

Algorithms	EASS	CLM4	DLM
Canopy layers	Two layers (overstory and understory)	One layer	Two layers (overstory and understory)
Snow layers	depending on snow depth	depending on snow depth	depending on snow depth
Soil layers	7	15	15
Canopy up-scaling	two-leaf strategy	one-leaf strategy	two-leaf strategy
Two-leaf (sunlit and shaded leaves) strategy implementation	based on fractions of sunlit and shaded leaves at a canopy depth as described by Dai et al.,(2004), also depending on the clumping index related of PFTs	based on fractions of sunlit and shaded leaves at a canopy depth as described by Dai et al.,(2004)	based on fractions of sunlit and shaded leaves at a canopy depth as described by Dai et al., (2004), also depending on the clumping index related of PFTs
Photosynthesis	two-leaf strategy, Rubisco-limited rate and light-limited rate are both based on Chen et al., (1999) and Wang and Leuning, (1998)	two-leaf strategy, Rubisco-limited rate and light-limited rate are both based on Bonan et al.,(2011)	two-leaf strategy, Rubisco-limited rate and light-limited rate are both based on Chen et al., (1999) and Wang and Leuning, (1998)
Evapo-transpiration	two-leaf strategy, Penman-Monteith equation	one-leaf strategy, Mass-transfer equation	two-leaf strategy, Penman-Monteith equation
Land cover type	6 vegetation types, burned area, barren land, urban area and permanent snow/ice area	15 possible PFTs, bare ground, crop, lake, urban and glacier	15 possible PFTs, bare ground, crop, lake, urban and glacier
Phenology	derived from leaf area index (LAI)	growing degree days (GDDs) model accompanying with day length and soil moisture restriction	growing season index(GSI) model
Vegetation carbon pools	as a whole	leaf, live stem, dead stem, live coarse root, dead coarse root, fine root, storage organs and respiration organs	leaf, live stem, dead stem, live coarse root, dead coarse root, fine root, storage organs and respiration organs
Litter carbon pools	Coarse detritus from woody and coarse root, surface structural litter, surface metabolic litter, surface microbe pool	coarse woody debris (CWD), 3 litter pools	coarse woody debris (CWD), 3 litter pools

Biogeosciences Discuss., doi:10.5194/bg-2016-165, 2016
Manuscript under review for journal Biogeosciences
Published: 29 April 2016

Soil carbon pools	soil structural litter pool, soil metabolic pool, soil microbe pool, slow carbon pool, passive carbon pool	4 soil organic matter pools	4 soil organic matter pools
Reference	(Chen et al. 2007; Chen et al. 1999; Dai et al. 2004; Wang; Leuning 1998)	(Bonan et al. 2011; Dai et al. 2004; Lawrence et al. 2011; Oleson et al. 2013; Oleson 2010; Thornton; Zimmermann 2007; Thornton et al. 2002; White et al. 1997)	(Chen et al. 2007; Chen et al. 2013; Chen et al. 1999; Dai et al. 2004; Jolly et al. 2005; Oleson et al. 2013; Oleson 2010; Stöckli et al. 2008; Wang; Leuning 1998)

Biogeosciences Discuss., doi:10.5194/bg-2016-165, 2016
Manuscript under review for journal Biogeosciences
Published: 29 April 2016

Table 2. Descriptions of global FLUXNET sites used.

NO.	Site ID[a]	Lon. (˚E)	Lat. (˚N)	Elev. (m)	Biome Type[b]	Climate Zone	Air Temp. (ºC yr^{-1})	Percip. (mm yr^{-1})	SiteYear
1	CA-NS1	-98.48	55.88	253	NDF	Boreal (Moist)	0.59	201.40	2002-2005
2	CA-Oas	-106.20	53.63	580	NDF	Boreal (Moist)	1.95	541.75	2003-2006
3	FI-Hyy	24.30	61.85	185	NDF	Boreal (Moist)	4.59	499.08	2004-2007
4	CH-Lae	8.37	47.48	689	BDF	Cool Temperate (Moist)	7.73	846.40	2005-2006, 2008-2009
5	FR-Fon	2.78	48.48	100	BDF	Warm Temperate (Dry)	11.35	668.08	2005-2008
6	IT-Col	13.59	41.85	1560	BDF	Warm Temperate (Moist)	7.44	994.04	2003-2006
7	US-Los	-89.98	46.08	485	BDF	Cool Temperate (Moist)	5.10	694.82	2001-2004
8	US-MOz	-92.20	38.74	212	BDF	Warm Temperate (Moist)	14.00	699.00	2004-2007
9	BE-Vie	6.00	50.31	450	BDF	Boreal (Moist)	8.36	1070.09	2005-2008
10	DE-Gri	13.51	50.95	385	BDF	Boreal (Moist)	8.72	874.33	2005-2008
11	DE-Hai	10.45	51.08	430	BDF	Boreal (Moist)	8.23	801.50	2004-2007
12	DK-Sor	11.65	55.49	40	BDF	Boreal (Moist)	8.54	658.86	2003-2006
13	CA-Mer	-75.52	45.41	65	BDS	Cool Temperate (Moist)	6.26	1048.18	2005-2008
14	US-Fwf	-111.77	35.45	2316	BDS	Cool Temperate (Dry)	8.63	895.78	2005-2008
15	US-Ton	-120.97	38.43	170	BDS	Warm Temperate (Dry)	16.32	535.86	2002-2003, 2006-2007
16	CA-NS6	-98.96	55.92	271	BDS	Boreal (Moist)	-0.86	256.05	2002-2005
17	US-Ivo	-155.75	68.49	557	BDS	Boreal (Moist)	-9.11	292.99	2003-2006
18	AT-Neu	11.32	47.12	970	GRA	Cool Temperate (Moist)	6.52	718.35	2003-2006
19	FI-Kaa	27.30	69.14	155	GRA	Cool Temperate (Moist)	0.46	459.73	2000-2001, 2004-2005
20	PT-Mi2	-8.03	38.48	190	GRA	Warm Temperate (Dry)	14.21	575.69	2005-2008
21	US-FPe	-105.10	48.31	638	GRA	Cool Temperate (Dry)	5.79	428.60	2003-2006
22	US-Wkg	-109.94	31.74	1524	GRA	Warm Temperate (Dry)	17.25	245.78	2004-2007

[a] The site ID is taken from FLUXNET.

[b] Biome types: needleleaf deciduous forest (NDF), broadleaf deciduous forest (BDF), broadleaf deciduous shrub (BDS), and grassland (GRA).

Biogeosciences Discuss., doi:10.5194/bg-2016-165, 2016
Manuscript under review for journal Biogeosciences
Published: 29 April 2016

Table 3. Phenological parameters in the DLM-GSI model[a]

Biome type	Climate zone	DL_{max} (hr)	DL_{min} (hr)	T_{max} (K)	T_{min} (K)	VPD_{max} (Pa)	VPD_{min} (Pa)	$GSIG_{thr}$ -	$GSID_{thr}$ -	N_{onset} (day)	N_{offset} (day)
NDF	Boreal	11.50	10.75	273	267	2113	886	0.5	0.5	37	32
BDF	Temperate	11.50	10.50	280	277	3084	899	0.5	0.5	31	32
BDF	Boreal	11.50	10.50	282	270	2095	916	0.5	0.5	36	17
BDS	Temperate	11.25	9.25	276	272	3199	912	0.5	0.5	27	28
BDS	Boreal	11.50	10.50	281	270	2100	903	0.5	0.5	32	31
GRA(C3)	Temperate	10.25	9.25	278	268	2270	700	0.5	0.5	27	30
Average[b]		11.25	10.13	278	271	2477	869	0.5	0.5	31	28

[a]parameters: the maximum day length threshold (DL_{max}), the minimum day length threshold (DL_{min}), the maximum air temperature threshold ($T_{\max}$), the minimum air temperature threshold ($T_{\min}$), the maximum vapor pressure deficit threshold (VPD_{max}), the minimum vapor pressure deficit threshold (VPD_{min}), the threshold for triggering the vegetation green-up ($GSIG_{thr}$), the threshold for triggering the vegetation defoliation ($GSID_{thr}$), the initialized onset counters for controlling the green-up length (N_{onset}), and the initialized offset counters for controlling the defoliation length (N_{offset}).

[b]Average was calculated for all biome types and climate zones.

Biogeosciences Discuss., doi:10.5194/bg-2016-165, 2016
Manuscript under review for journal Biogeosciences
Published: 29 April 2016

Table 4. Comparison of the root mean square error (RMSE) and the index of agreements (IAs) for gross primary production simulation for different vegetation types using the DLM-GSI and DLM-GDD models.

Biome type Climate zone	RMSE (gC m^{-2} d^{-1})		IA	
	DLM-GSI	DLM-GDD	DLM-GSI	DLM-GDD
NDF Boreal	2.055	2.197	0.830	0.799
BDF Temp.	2.759	2.817	0.842	0.838
BDF Boreal	3.399	3.523	0.846	0.830
BDS Temp.	1.420	1.689	0.786	0.696
BDS Boreal	0.764	1.035	0.858	0.742
GRA Temp.	1.349	1.642	0.733	0.619
Average	2.095	2.278	0.810	0.753

Biogeosciences Discuss., doi:10.5194/bg-2016-165, 2016
Manuscript under review for journal Biogeosciences
Published: 29 April 2016

Figures caption

Figure 1. Methodology for extracting phenophases in GSI module.

Figure 2. Spatial distribution of global FLUXNET sites.

Figure 3. Example images of the canopy phenological changes at the US-MOz site.

Figure 4. Comparison of simulated phenophases by using the DLM-GSI and DLM-GDD models with the observations derived from the green chromatic coordinate (GCC) data at the US-MOz site.

Figure 5. Absolute bias comparison between simulated phenophases using the DLM-GSI and DLM-GDD models at the US-MOz site.

Figure 6. Comparison of simulated phenophases using the DLM-GSI and the DLM-GDD models with the observations derived from the eddy-covariance measured gross primary production data at all sites.

Figure 7. Absolute bias comparison between simulated phenophases using the DLM-GSI and the DLM-GDD models at all sites.

Figure 8. A boxplot of absolute biases for phenophases simulated using the DLM-GSI and DLM-GDD models.

Figure 9. Comparison of simulated gross primary production using the DLM-GSI and DLM-GDD models with the observations at all sites.

Figure 10. Histogram comparison of the root mean square error (RMSE) and the index of agreement (IA) for gross primary production simulation using the

Biogeosciences Discuss., doi:10.5194/bg-2016-165, 2016
Manuscript under review for journal Biogeosciences
Published: 29 April 2016

DLM-GSI and DLM-GDD models.

Figure 11. Influence of phenological parameters sensitivity on the growing season index (GSI) varying (US-Wkg, 2007).

Biogeosciences Discuss., doi:10.5194/bg-2016-165, 2016
Manuscript under review for journal Biogeosciences
Published: 29 April 2016

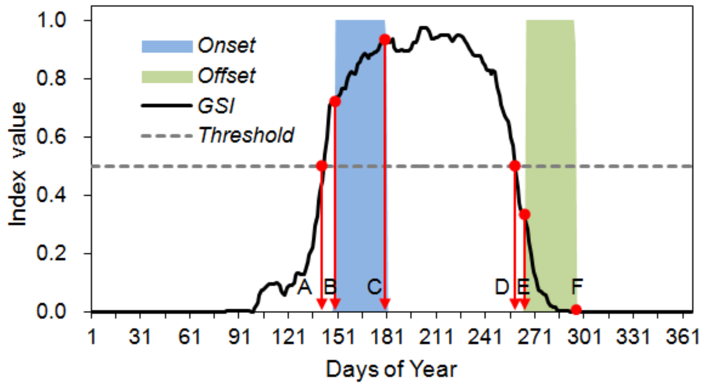

Figure 1. Methodology for extracting phenophases in GSI module. The italics '*Onset*' and '*Offset*' represent the period of green-up and the period of defoliation, respectively. The italics '*GSI*' and '*Threshold*' represent the growing season index and the threshold of GSI, respectively. The letter 'B, C, E, F' represents the green-up, the normal growth, the defoliation and the dormancy, respectively. The letter 'A' and 'D' represents the trgger point of green-up and the trgger point of defoliation, respectively.

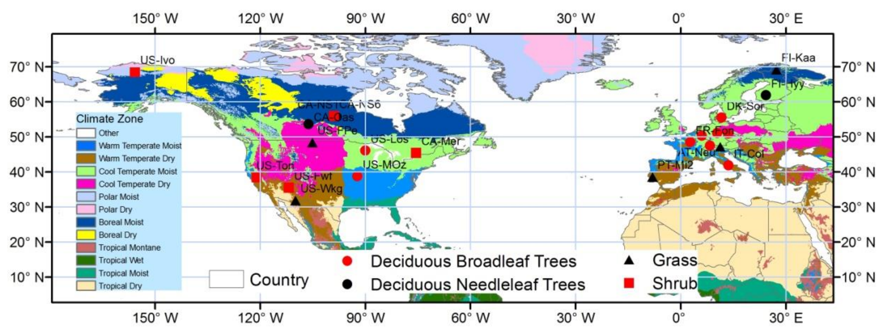

Figure 2. Spatial distribution of global FLUXNET sites.

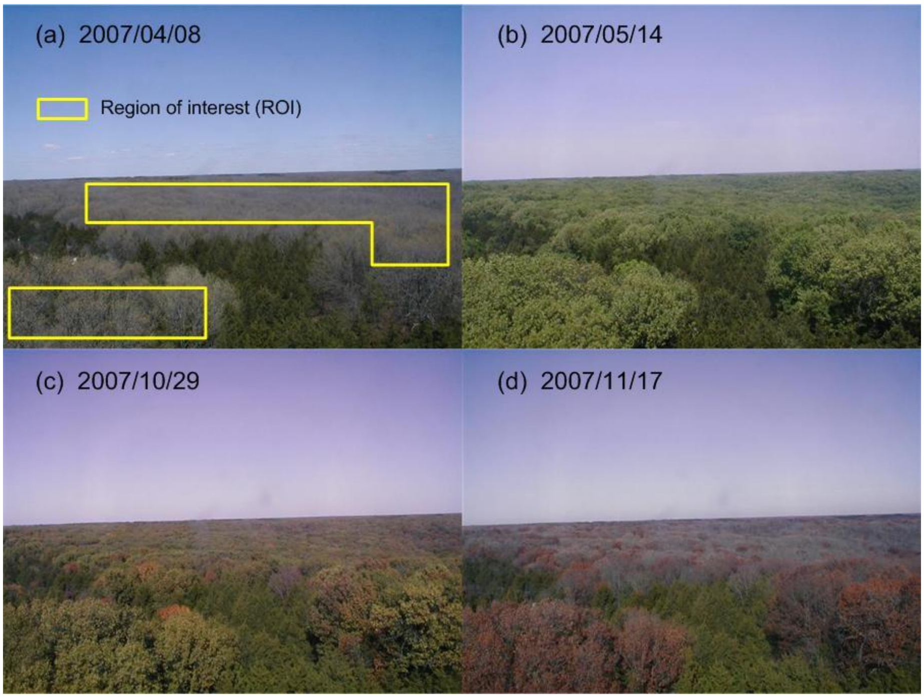

Figure 3. Example images of the canopy phenological changes at the US-MOz site. The vegetation type in the ROI is the broad-leaf deciduous forest. The letter 'a-d' represents the green-up, the normal growth, the defoliation and the dormancy, respectively.

Biogeosciences Discuss., doi:10.5194/bg-2016-165, 2016
Manuscript under review for journal Biogeosciences
Published: 29 April 2016

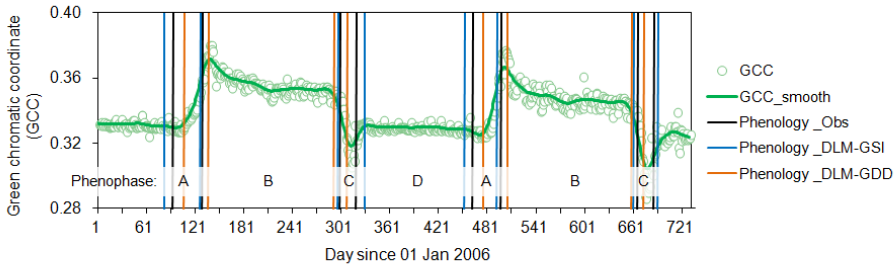

Figure 4. Comparison of simulated phenophases by using the DLM-GSI and DLM-GDD models with the observations derived from the green chromatic coordinate (GCC) data at the US-MOz site.

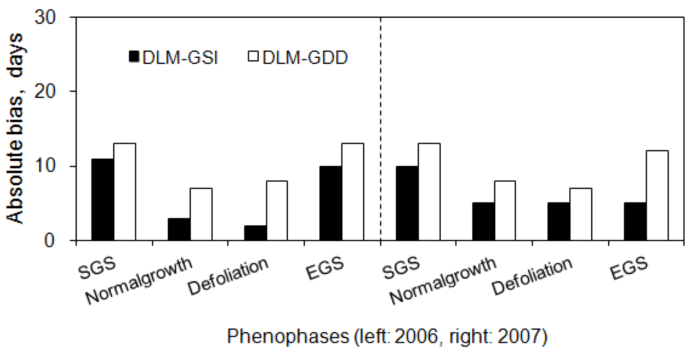

Figure 5. Absolute bias comparison between simulated phenophases using the DLM-GSI and DLM-GDD models at the US-MOz site. The abbr. ‘SGS’ represents the start of growing season, and the ‘EGS’ means the end of growing season.

Biogeosciences Discuss., doi:10.5194/bg-2016-165, 2016
Manuscript under review for journal Biogeosciences
Published: 29 April 2016

Biogeosciences Discussions
Open Access

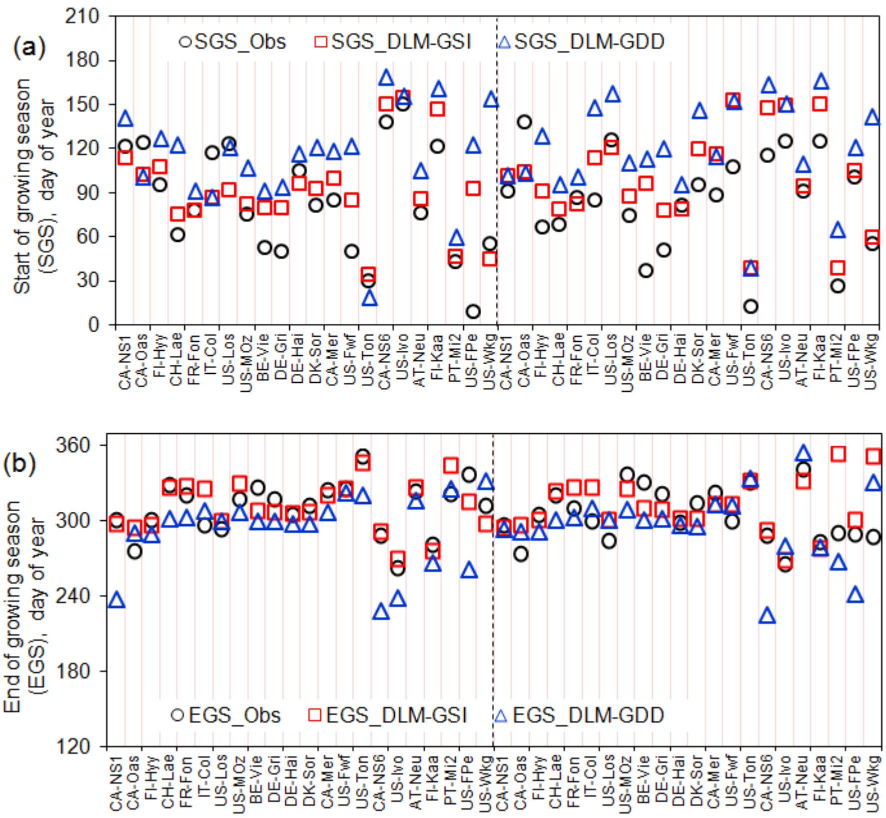

Figure 6. Comparison of simulated phenophases using the DLM-GSI and the DLM-GDD models with the observations derived from the eddy-covariance measured gross primary production data at all sites. The letters 'a' and 'b' represent the start of growing season (SGS) and the end of growing season (EGS), respectively. All sites in each subfigure contain two consecutive years.

Biogeosciences Discuss., doi:10.5194/bg-2016-165, 2016
Manuscript under review for journal Biogeosciences
Published: 29 April 2016

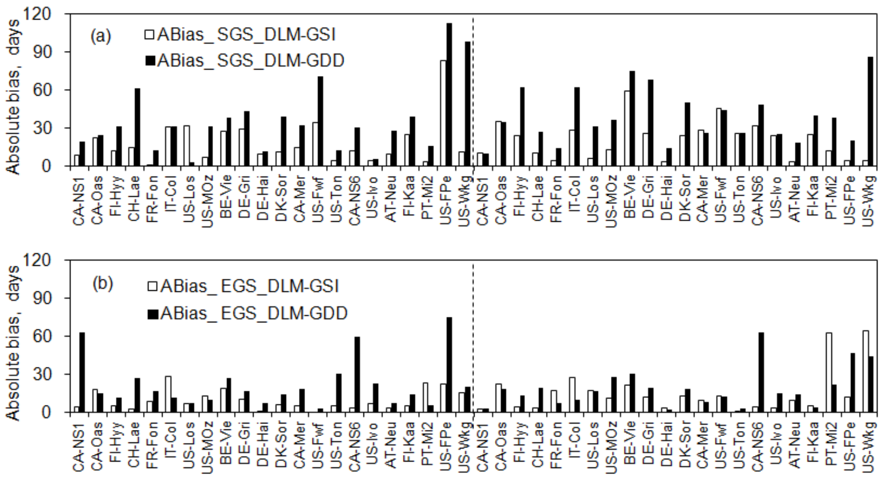

Figure 7. Absolute bias comparison between simulated phenophases using the DLM-GSI and the DLM-GDD models at all sites. The letters 'a' and 'b' represent the start of growing season (SGS) and the end of growing season (EGS), respectively. All sites in each subfigure contain two consecutive years.

Biogeosciences Discuss., doi:10.5194/bg-2016-165, 2016
Manuscript under review for journal Biogeosciences
Published: 29 April 2016

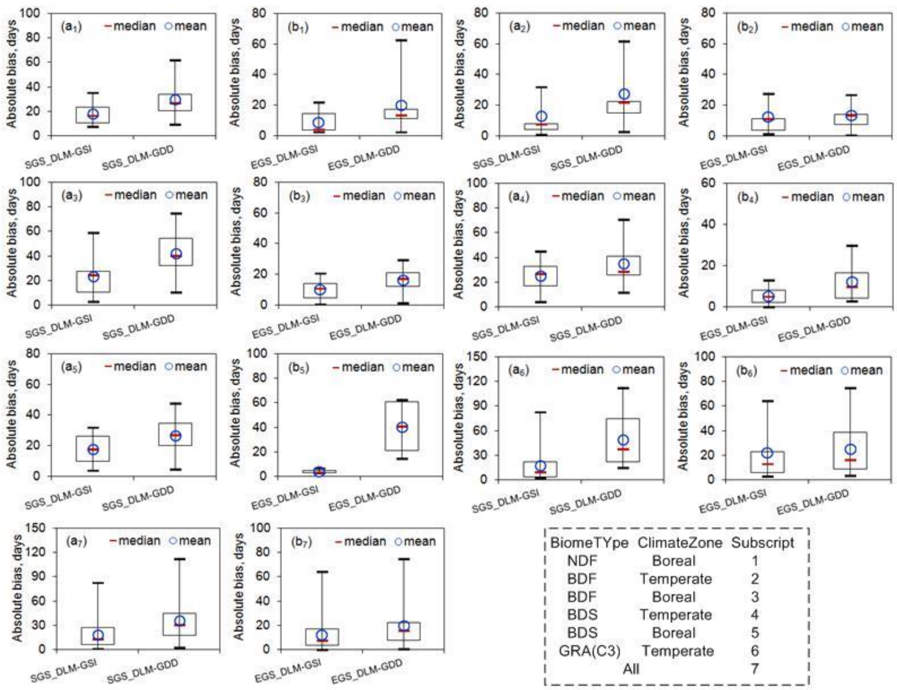

Figure 8. A boxplot of absolute biases for phenophases simulated using the DLM-GSI and DLM-GDD models. The letters ‘a’ and ‘b’ represent the start of growing season (SGS) and the end of growing season (EGS), respectively. The abbreviations in the biome types: ‘NDF’ represents needleleaf deciduous forest; ‘BDF’ represents broadleaf deciduous forest; ‘BDS’ represents broadleaf deciduous shrub; ‘GRA’ represents grassland.

Biogeosciences Discuss., doi:10.5194/bg-2016-165, 2016
Manuscript under review for journal Biogeosciences
Published: 29 April 2016

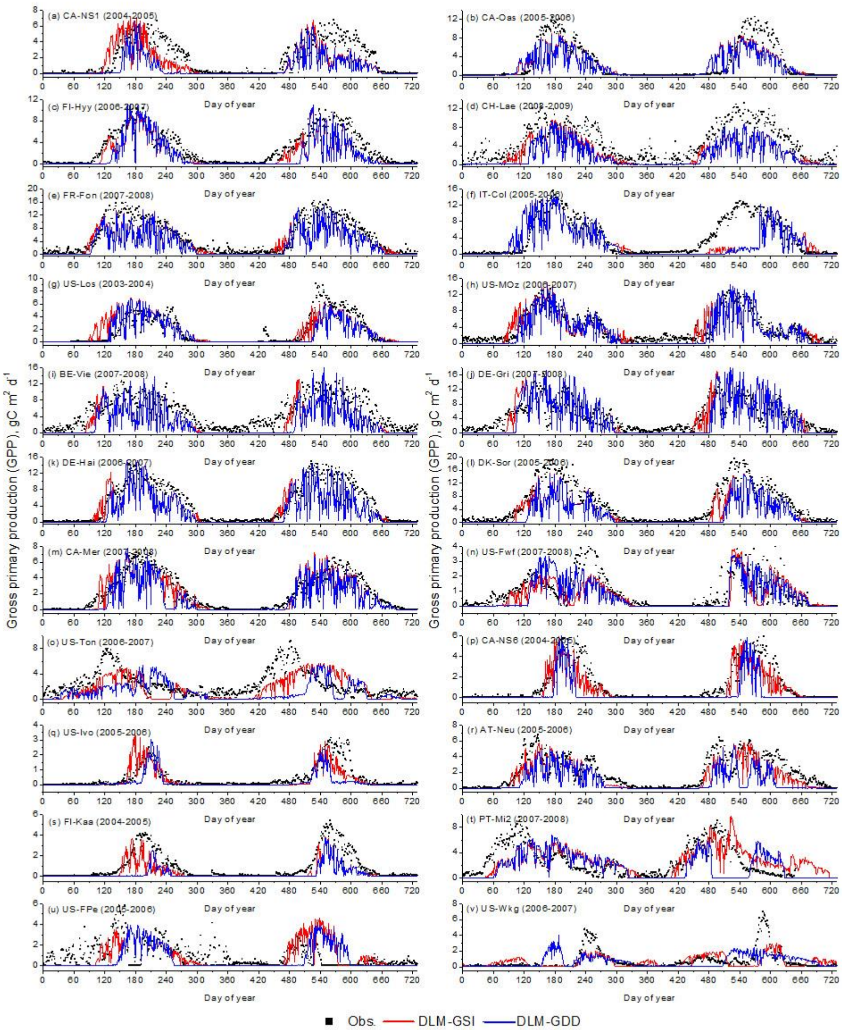

Figure 9. Comparison of simulated gross primary production using the DLM-GSI and DLM-GDD models with the observations at all sites.

Biogeosciences Discuss., doi:10.5194/bg-2016-165, 2016
Manuscript under review for journal Biogeosciences
Published: 29 April 2016

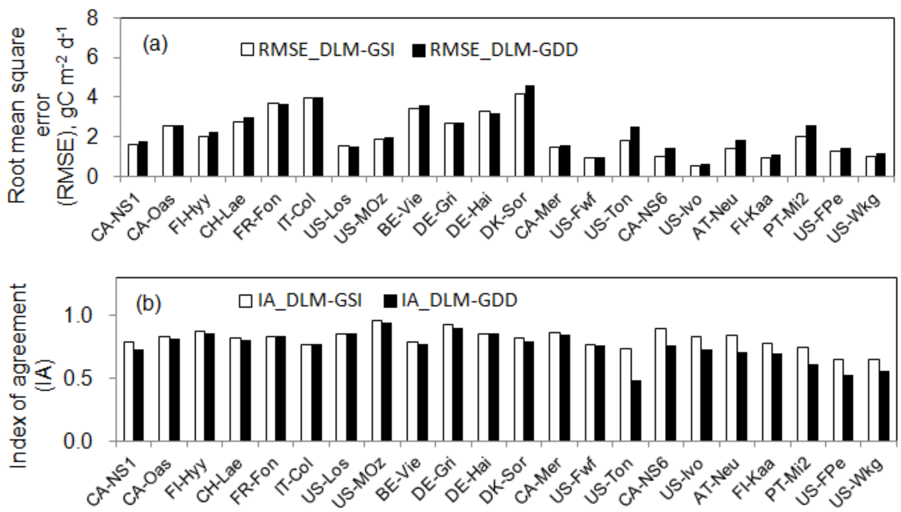

Figure 10. Histogram comparison of the root mean square error (RMSE) and the index of agreement (IA) for gross primary production simulation using the DLM-GSI and DLM-GDD models. The letters 'a' and 'b' represent the RMSE and IA, respectively.

Biogeosciences Discuss., doi:10.5194/bg-2016-165, 2016
Manuscript under review for journal Biogeosciences
Published: 29 April 2016

800 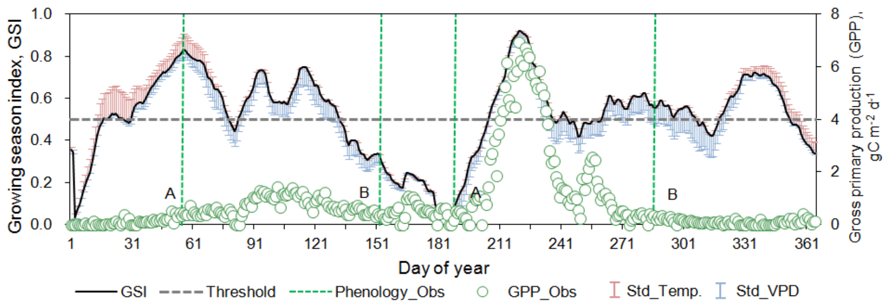

801 Figure 11. Influence of phenological parameters sensitivity on the growing season
802 index (GSI) varying (US-Wkg, 2007). The error bars in light red being marked as
803 positive errors were the sensitivity standard deviation of the temperature. The
804 error bars in light blue being marked as negative errors were the sensitivity
805 standard deviation of the vapor pressure deficit (VPD). The letters A and B
806 represent the start of growing season and the end of growing season, respectively.
807 The observed phenophases data were derived from the eddy-covariance
808 measured gross primary production (GPP).

809

810

Biogeosciences Discuss., doi:10.5194/bg-2016-165, 2016
Manuscript under review for journal Biogeosciences
Published: 29 April 2016

References

Ahrends, H. E., and Coauthors, 2008: Quantitative phenological observations of a mixed beech forest in northern Switzerland with digital photography. *Journal of Geophysical Research*, **113**.

Ahrends, H. E., and Coauthors, 2009: Tree phenology and carbon dioxide fluxes: use of digital photography for process-based interpretation at the ecosystem scale. *Climate Research*, **39,** 261-274.

Arora, V. K., and G. J. Boer, 2005: A parameterization of leaf phenology for the terrestrial ecosystem component of climate models. *Global Change Biology*, **11,** 39-59.

Bonan, G. B., and Coauthors, 2011: Improving canopy processes in the Community Land Model version 4 (CLM4) using global flux fields empirically inferred from FLUXNET data. *Journal of Geophysical Research*, **116**.

Borchert, R., K. Robertson, M. D. Schwartz, and G. Williams-Linera, 2005: Phenology of temperate trees in tropical climates. *International journal of biometeorology*, **50,** 57-65.

Caffarra, A., A. Donnelly, I. Chuine, and M. B. Jones, 2011: Modelling the timing of Betula pubescens budburst. I. Temperature and photoperiod: a conceptual model. *Climate Research*, **46,** 147-157.

Che, M., B. Chen, H. Zhang, S. Fang, G. Xu, X. Lin, and Y. Wang, 2014a: A New

Biogeosciences Discuss., doi:10.5194/bg-2016-165, 2016
Manuscript under review for journal Biogeosciences
Published: 29 April 2016

Equation for Deriving Vegetation Phenophase from Time Series of Leaf Area Index (LAI) Data. *Remote Sensing*, **6,** 5650-5670.

Che, M., and Coauthors, 2014b: Spatial and temporal variations in the end date of the vegetation growing season throughout the Qinghai–Tibetan Plateau from 1982 to 2011. *Agricultural and Forest Meteorology*, **189-190,** 81-90.

Chen, B., J. M. Chen, and W. Ju, 2007: Remote sensing-based ecosystem-atmosphere simulation scheme (EASS) - Model formulation and test with multiple-year data. *Ecological Modelling*, **209,** 277-300.

Chen, J., H. Zhang, Z. Liu, M. Che, and B. Chen, 2014: Evaluating Parameter Adjustment in the MODIS Gross Primary Production Algorithm Based on Eddy Covariance Tower Measurements. *Remote Sensing*, **6,** 3321-3348.

Chen, J., and Coauthors, 2013: Comparison of terrestrial evapotranspiration estimates using the mass transfer and Penman-Monteith equations in land surface models. *Journal of Geophysical Research: Biogeosciences*, **118,** 1715-1731.

Chen, J. M., J. Liu, J. Cihlar, and M. L. Goulden, 1999: Daily canopy photosynthesis model through temporal and spatial scaling for remote sensing applications. *Ecological Modelling*, **124,** 99-119.

Chuine, I., 2000: A unified model for the budburst of trees. *J. Theor. Biol.*, **207,** 337-347.

Cong, N., T. Wang, H. J. Nan, Y. C. Ma, X. H. Wang, R. B. Myneni, and S. L. Piao, 2012: Changes in satellite-derived spring vegetation green-up date and its linkage to climate in China from 1982 to 2010: a multimethod analysis. *Global Change Biology*, **19,** 881-891.

Dai, Y. J., R. E. Dickinson, and Y. P. Wang, 2004: A two-big-leaf model for canopy temperature, photosynthesis, and stomatal conductance. *Journal of Climate*, **17,** 2281-2299.

Dong, Y., C. Zhao, G. Yang, L. Chen, J. Wang, and H. Feng, 2013: Integrating a very fast simulated annealing optimization algorithm for crop leaf area index variational assimilation. *Mathematical and Computer Modelling*, **58,** 877-885.

Eastman, J., F. Sangermano, E. Machado, J. Rogan, and A. Anyamba, 2013: Global Trends in Seasonality of Normalized Difference Vegetation Index (NDVI), 1982–2011. *Remote Sensing*, **5,** 4799-4818.

Foley, J. A., I. C. Prentice, N. Ramankutty, S. Levis, D. Pollard, S. Sitch, and A. Haxeltine, 1996: An integrated biosphere model of land surface processes, terrestrial carbon balance, and vegetation dynamics. *Global Biogeochemical Cycles*, **10,** 603-628.

Hamunyela, E., J. Verbesselt, G. Roerink, and M. Herold, 2013: Trends in Spring Phenology of Western European Deciduous Forests. *Remote Sensing*, **5,** 6159-6179.

Ide, R., and H. Oguma, 2010: Use of digital cameras for phenological observations. *Ecological Informatics*, **5,** 339-347.

Jolly, W. M., R. Nemani, and S. W. Running, 2005: A generalized, bioclimatic index

Biogeosciences Discuss., doi:10.5194/bg-2016-165, 2016
Manuscript under review for journal Biogeosciences
Published: 29 April 2016

to predict foliar phenology in response to climate. *Global Change Biology*, **11,** 619-632.

Klosterman, S. T., and Coauthors, 2014: Evaluating remote sensing of deciduous forest phenology at multiple spatial scales using PhenoCam imagery. *Biogeosciences*, **11,** 4305-4320.

Knorr, W., T. Kaminski, M. Scholze, N. Gobron, B. Pinty, R. Giering, and P. P. Mathieu, 2010: Carbon cycle data assimilation with a generic phenology model. *Journal of Geophysical Research*, **115**.

Kucharik, C. J., 2003: Evaluation of a Process-Based Agro-Ecosystem Model (Agro-IBIS) across the US Corn Belt: Simulations of the Interannual Variability in Maize Yield. *Earth Interact*, **7,** 1-14.

Kucharik, C. J., and T. E. Twine, 2007: Residue, respiration, and residuals: Evaluation of a dynamic agroecosystem model using eddy flux measurements and biometric data. *Agricultural and Forest Meteorology*, **146,** 134-158.

Lawrence, D. M., and Coauthors, 2011: Parameterization improvements and functional and structural advances in Version 4 of the Community Land Model. *Journal of Advances in Modeling Earth Systems*, **3**.

Li, X., T. Koike, and M. Pathmathevan, 2004: A very fast simulated re-annealing (VFSA) approach for land data assimilation. *Computers & Geosciences*, **30,** 239-248.

Ludvig, F., 2014: Using digital repeat photography for monitoring the regrowth of a clear-cut area, Department of Physical Geography and Ecosystems Science, Lund University.

Melaas, E. K., and Coauthors, 2013: Using FLUXNET data to improve models of springtime vegetation activity onset in forest ecosystems. *Agricultural and Forest Meteorology*, **171-172,** 46-56.

Menzel, A., and P. Fabian, 1999: Growing season extended in Europe. *Nature*, **397,** 659.

Monteith, J. L., 1972: Solar Radiation and Productivity in Tropical Ecosystems. *Journal of Applied Ecology*, **9,** 747-766.

Murray, M. B., G. R. Cannell, and R. I. Smith, 1989: Date of budburst of fifteen tree species in Britain following climatic warming. *J. Appl. Ecol.*, **26,** 693-700.

Oleson, K. W., and Coauthors, 2013: Technical Description of version 4.5 of the Community Land Model (CLM). National Center for Atmospheric Research: Boulder.

Oleson, K. W., and Coauthors, 2010: *Technical Description of version 4.0 of the Community Land Model (CLM).* National Center for Atmospheric Research.

Oleson, K. W. L., D.M.; Bonan, G.B.; Flanner, M.G.; Kluzek, E.; Lawrence, P.J.; Levis, S.; Swenson, S.C.; Thornton, P.E.; Dai, A., et al., 2010: Technical Description of version 4.0 of the Community Land Model (CLM). National Center for Atmospheric Research.

Qian, T., A. Dai, K. E. Trenberth, and O. K. W., 2006: Simulation of Global Land

Surface Conditions from 1948 to 2004. Part I: Forcing Data and Evaluations. *Journal of Hydrometeorology*, **7,** 953-974.

Roth, K. L., D. A. Roberts, P. E. Dennison, S. H. Peterson, and M. Alonzo, 2015: The impact of spatial resolution on the classification of plant species and functional types within imaging spectrometer data. *Remote Sensing of Environment*, **171,** 45-57.

Schaefer, K., and Coauthors, 2012: A model-data comparison of gross primary productivity: Results from the North American Carbon Program site synthesis. *Journal of Geophysical Research*, **117**.

Schwartz, M. D., 1998: Green-wave phenology. *Nature*, **394,** 839-840.

——, 2013: *Phenology: An Integrative Environmental Science.* Second ed. Springer Dordrecht Heidelberg.

Sims, D., and Coauthors, 2008: A new model of gross primary productivity for North American ecosystems based solely on the enhanced vegetation index and land surface temperature from MODIS. *Remote Sensing of Environment*, **112,** 1633-1646.

Sitch, S., and Coauthors, 2000: *LPJ-A Coupled Model of Vegetation Dynamics and the Terrestrial Carbon Cycle.* The Role of Vegetation Dynamics in the Control of Atmospheric CO2 Content, Ph.D. Thesis.

Sitch, S., and Coauthors, 2003: Evaluation of ecosystem dynamics, plant geography and terrestrial carbon cycling in the LPJ dynamic global vegetation model.

Global Change Biology, **9,** 161-185.

Sonnentag, O., and Coauthors, 2012: Digital repeat photography for phenological research in forest ecosystems. *Agricultural and Forest Meteorology*, **152,** 159-177.

Stöckli, R., and Coauthors, 2008: Remote sensing data assimilation for a prognostic phenology model. *Journal of Geophysical Research*, **113**.

Subin, Z. M., W. J. Riley, J. Jin, D. S. Christianson, M. S. Torn, and L. M. Kueppers, 2011: Ecosystem Feedbacks to Climate Change in California: Development, Testing, and Analysis Using a Coupled Regional Atmosphere and Land Surface Model (WRF3–CLM3.5). *Earth Interact*, **15,** 1-38.

Thornton, P. E., and N. A. Rosenbloom, 2005: Ecosystem model spin-up: Estimating steady state conditions in a coupled terrestrial carbon and nitrogen cycle model. *Ecological Modelling*, **189,** 25-48.

Thornton, P. E., and N. E. Zimmermann, 2007: An Improved Canopy Integration Scheme for a Land Surface Model with Prognostic Canopy Structure. *Journal of Climate*, **20,** 3902-3923.

Thornton, P. E., and Coauthors, 2002: Modeling and measuring the effects of disturbance history and climate on carbon and water budgets in evergreen needleleaf forests. *Agricultural and Forest Meteorology*, **113,** 185-222.

Wang, Y.-P., and R. Leuning, 1998: A two-leaf model for canopy conductance, photosynthesis and partitioning of available energy I: Model description and

Biogeosciences Discuss., doi:10.5194/bg-2016-165, 2016
Manuscript under review for journal Biogeosciences
Published: 29 April 2016

comparison with a multi-layered model. *Agricultural and Forest Meteorology*, **91,** 89-111.

White, K., J. Pontius, and P. Schaberg, 2014: Remote sensing of spring phenology in northeastern forests: A comparison of methods, field metrics and sources of uncertainty. *Remote Sensing of Environment*, **148,** 97-107.

White, M. A., P. E. Thornton, and S. W. Running, 1997: A continental phenology model for monitoring vegetation responses to interannual climatic variability. *Global Biogeochemical Cycels*, **11,** 217-234.

White, M. A., and Coauthors, 2009: Intercomparison, interpretation, and assessment of spring phenology in North America estimated from remote sensing for 1982-2006. *Global Change Biology*, **15,** 2335-2359.

Willmott, C. J., 1982: Some Comments on the Evaluation of Model Performance. *Bulletin American Meteorological Society*, **63,** 1309-1313.

Zeng, X., F. Li, and X. Song, 2014: Development of the IAP Dynamic Global Vegetation Model. *Advances in Atmospheric Sciences*, **31,** 505-514.